연구논문

J Korean Soc Fluid Power Constr Equip Vol.9 No.4 pp.42-51 Dec. 2012
ISSN(print) 2234-8328 ISSN(online) 2287-6146
http://dx.doi.org/10.7839/ksfc.2012.9.4.042

엔진오일용 가변 베인펌프의 수학적 모델 개발
Development of a mathematic model for a variable displacement vane pump for engine oil

딩광청[1] · 안경관[1*] · 윤종일[1] · 이재신[2]
D. Q. Truong, K. K. Ahn, J. I. Yoon and J. S. Lee

Received: 29 Aug. 2012, Revised: 23 Nov. 2012, Accepted: 28 Nov. 2012

Key Words : Engine Lubrication(엔진윤활), Vane Pump(베인펌프), Variable Displacement(가변용량), Modeling(모델링)

Abstract: Variable displacement vane-type oil pumps represent one of the most innovative pump types for industrial applications, especially for engine lubrication systems. This paper deals with a modeling method for theoretical flow rate investigation of a typical variable displacement vane-type oil pump. This theoretical model is based on the pump geometric design and dynamic analyses. It can be considered as mandatory steps for a deeper understanding of the pump operation as well as for effectively implementing the pump control mechanisms to satisfy the urgent demands of engine lubrication systems. The developed pump model is finally illustrated by numerical simulations.

1. 서 론

Nowadays, the design requirements for engine lubrication systems, especially for vehicle applications, have been oriented to a general performance improvement, coupled with a contemporary reduction of power losses, weights and volumes. A fixed displacement lubricating pump driven by a rotating component of the mechanical system is generally designed to operate effectively at a target speed and a maximum operating lubricant temperature. Meanwhile, the lubrication requirements of the machine do not directly correspond to its operating speed. It results in an oversupply of lubricating oil at most machines. A pressure relief valve is then provided to return the surplus lubricating oil back into the pump inlet or a reservoir to avoid over pressure conditions in the mechanical system. The result is a significant amount of energy being used to pressurize the lubricating oil which is subsequently exhausted through the relief valve. Subsequently, a potential trend for machine lubrication is the employment of variable displacement vane pumps as lubrication oil pumps. To vary the displacement, there are two common approaches which are the use of a linear translating cam ring[1-3], and the use of a pivoting cam ring[4-12]. By the second method, each pump of these types generally includes a control ring combined with other mechanisms such as springs, which can be operated to alter the volumetric displacement of the pump and thus its output at an operating speed. The pump control mechanisms are normally supplied with pressurized lubricating oil from the pump output to drive the pump displacement and to avoid over pressure situations in the engine throughout the expected operating range of the mechanical system. Therefore, development of a variable displacement vane-type oil pump model is indispensable and can be considered as a priority task in order to investigate the

* Corresponding author: kkahn@ulsan.ac.kr
1 School of Mechanical Engineering, University of Ulsan, Ulsan, Korea.
2 School of Materials Science and Engineering, University of Ulsan, Ulsan, Korea.

pump working performance as well as to optimize the pump design structure. Some studies relating to this field have been done to investigate the pump performances[8-11]. Giuffrida and Lanzafame[8] derived a mathematical model for a fixed displacement balanced vane pump to analyze the theoretical flow rate through the cam shape design and vane thickness. Staley et al.[9] carried out a study on a variable displacement vane pump for engine lubrication. Loganathan et al.[10] also developed a variable displacement vane pump for automotive applications by simulations and experiments. In another study, Kim et al.[11] investigated an electronic control variable displacement lubrication oil pump through a simple mathematical model. Although these studies bring some interesting results, a clear and careful analysis of the theoretical flow rate in a variable displacement vane-type oil pump was not considered.

This paper is to develop a theoretical model of a typical variable displacement vane-type oil pump based on its geometric and dynamic analyses. By using this model, the ideal pump flow rate could be easily investigated through numerical simulations. It can be considered as mandatory steps for a deeper understanding of pump operation as well as for effectively implementing pump control mechanism to satisfy the urgent lubrication demands.

2. Model Design for A Typical Variable Displacement Vane Type Oil Pump

2.1 Variable Displacement vane type oil pump

In this study, a variable displacement vane-type oil pump made by MyungHwa Co. Ltd.[12] as displayed in Fig. 1 was used for the investigation. During the pump operation, the vanes slide out of the rotor slots and the vane tip-edges always contact with the ring inside contour due to their centrifugal effects. Subsequently, it performs pumping chambers between succeeding vanes to carry oil from the inlet to the outlet. The increase in volumes forming by pumping chambers allows the oil to be pushed in by atmospheric pressure from oil sump through suction pipe.

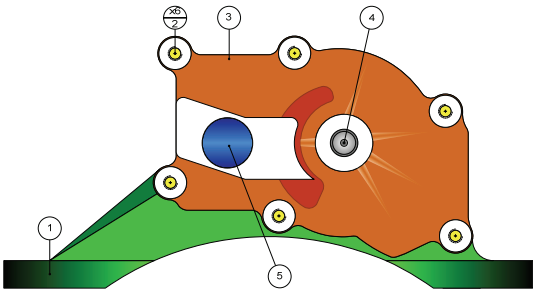

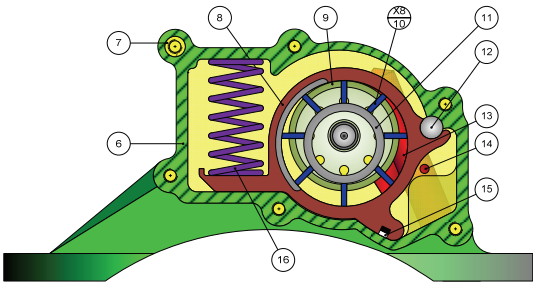

1 Base	6 Main-covered coat	11 Sub ring
2 Tapped holes	7 Located pin	12 Pivot pin
3 Sub-covered coat	8 Main ring	13 Deliver port
4 Drive shaft	9 Rotor	14 Orifice
5 Suction port	10 Vanes	15 Oil seals
		16 Spring

Fig. 1 Research vane type oil pump

The pumping chamber volumes continue to increase in size for the first half of each rotation. The oil is then carried to the other side where the pumping chamber volumes begin to be reduced. Finally, the oil is squeezed out at the outlet as the pumping chamber's size decreases.

For varying the pump displacement, rotation of the main ring around the pivot pin is controlled by pressured oil itself in the control chamber through the orifice, the pumping chambers, centrifugal force effects and the return spring.

2.2 Oil pump model design

2.2.1 Vane movement analysis

The analysis of a generic vane i^{th} is carried out on a cross section of the pump as in Fig. 2. Points O_r and O_s are in turn the centers of rotor and main ring inside surface of which their radiuses are R_r and R_s. The eccentricity between the rotor and the ring inner surface is e_c. There are N vanes with thickness t_v and radius R_v at its tip curve (center point O_{vi}). At the initial state, each vane stays at the end of the corresponding slot

defined by radius R_{rv}. Point Bi is the intersection point between the tip arc and center line of the vane.

The rotor rotates with a constant velocity ω (pump speed is n). At a current angular position of the rotor, α, position of the vane i^{th} can be defined as

$$\alpha_i = \alpha - \frac{2\pi}{N}(i-1),\ i = 1..N \tag{1}$$

Due to the centrifugal effect, the vane contacts with the inside surface of the main ring at point A_i. Point A_i is far from point B_i as an angle γ_i. Following relations can be obtained:

$$\rho_i = \sqrt{R_v^2 + \overline{O_r O_{vi}}^2 + 2R_v \overline{O_r O_{vi}} \cos\gamma_i},\ i = 1..N \tag{2}$$

$$\beta_i = \operatorname{acos}\frac{\rho_i^2 + e_c^2 - R_s^2}{2\rho_i e_c} \tag{3}$$

$$\gamma_i = \operatorname{asin}\left(\frac{e_c \sin\alpha_i}{R_s - R_v}\right) \tag{4}$$

$$\overline{O_r O_{vi}} = \sqrt{e_c^2 + (R_s - R_v)^2 + 2e_c(R_s - R_v)\cos(\alpha_i + \gamma_i)} \tag{5}$$

Subsequently, the vane lift (l_v) can be obtained as

$$l_{vi} = \overline{O_r B_i} - R_r = \overline{O_r O_{vi}} + R_v - R_r \tag{6}$$

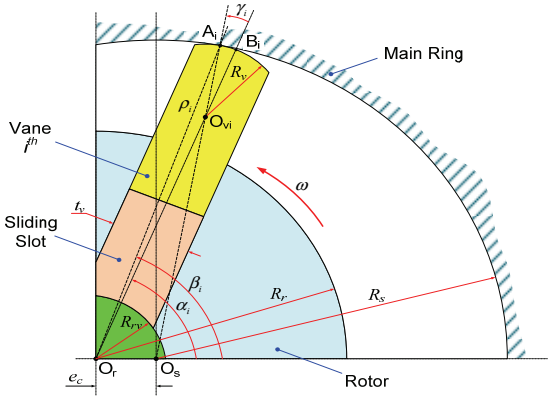

Fig. 2 Geometric analysis of a generic vane

2.2.2 Theoretical pump flow rate analysis

Fig. 3 displays the volume variation analysis for the chamber under the considered vane i^{th} corresponding to a small rotational angle of the rotor $d\alpha$. The volume derivative of the chamber under vane i^{th}, $dV_{uv}(\alpha_i)/d\alpha$, is computed as

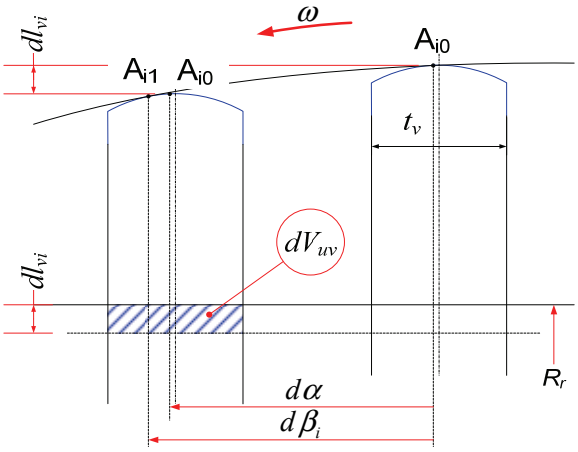

Fig. 3 Volume variation for a chamber under a generic vane

$$\frac{dV_{uv}(\alpha_i)}{d\alpha} = b \times t_v \times \frac{dl_v(\alpha_i)}{d\alpha} \equiv b \times t_v \times \frac{dl_{vi}}{d\alpha} \tag{7}$$

where: b is the ring depth.

Next, the volume variation for a chamber between two consecutive vanes (i^{th} and $(i+1)^{th}$) occupying the angular positions α_i and $\alpha_{i+1} \equiv \alpha_i + 2\pi/N$ respectively is analyzed in Fig. 4. This volume variation can be computed:

$$dV_{bv}(\alpha_i, \alpha_{i+1}) = dV_{bv\_in}(\alpha_i, \alpha_{i+1}) - dV_{bv\_out}(\alpha_i, \alpha_{i+1}) \tag{8}$$

After the small rotation $d\alpha$ of the rotor, the two vanes i^{th} and $(i+1)^{th}$ contact with the ring surface in turn at two points A_{i1} and $A_{(i+1)1}$ which are different from the previous ones (A_{i0} and $A_{(i+1)0}$). Consequently, it causes both of the input and output volumes to be reduced small amounts as marked as part S_{i2} in Fig. 4(b). Based on this figure and by a simple calculation, the volumes of oil entered into and pumped out of the chamber between two consecutive vanes can be in turn derived as in (9) and (10) (represented as part S_{i1} in Fig. 4(b):

$$dV_{bv\_in}(\alpha_i, \alpha_{i+1}) = \frac{1}{2}b\left(\rho_{i+1}^2 d\beta_{i+1} - \rho_{i+1}^2 d\theta_{i+1}\right) \tag{9}$$

$$dV_{bv\_out}(\alpha_i, \alpha_{i+1}) = \frac{1}{2}b\left(\rho_i^2 d\beta_i - \rho_i^2 d\theta_i\right) \tag{10}$$

$$d\theta_i = d\beta_i - d\alpha \tag{11}$$

From equations (8) to (11), the volume derivative of

the chamber between vanes is finally obtained as

$$\frac{dV_{bv}(\alpha_i,\alpha_{i+1})}{d\alpha}=\frac{b}{2}\left(\rho_{i+1}^2-\rho_i^2\right) \tag{12}$$

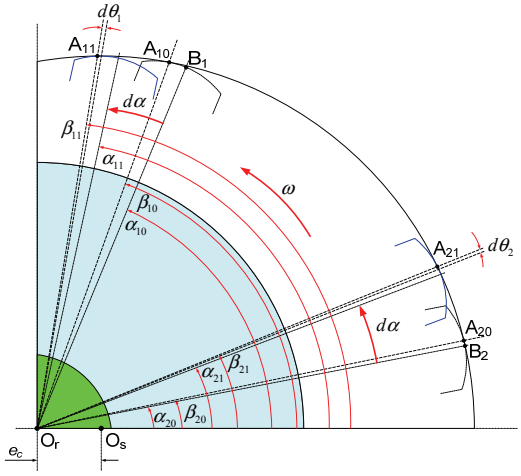

(a) Rotational analysis of 2 consecutive vanes

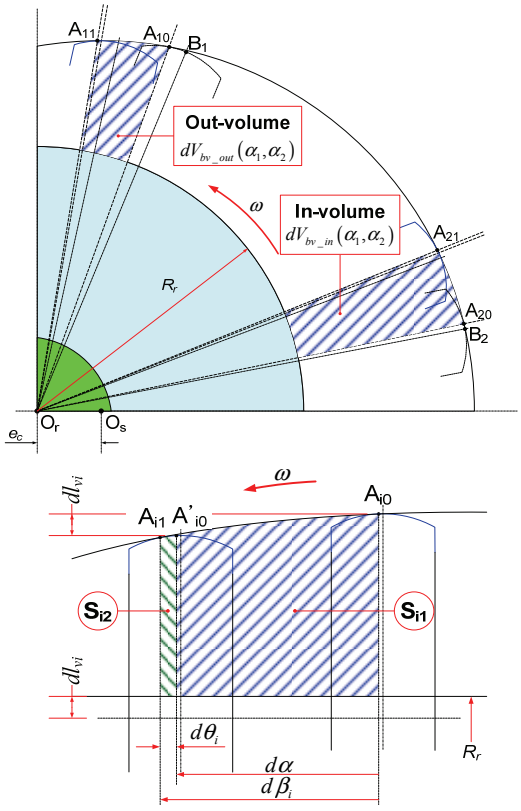

(b) In/out-volume analysis of a chamber between two consecutive vanes

Fig. 4 Volume variation for a chamber between two consecutive vanes

Finally, the ideal theoretical flow rate of the vane pump can be computed based on (7) and (12) as follows:

$$\begin{aligned}Q_{th}(\alpha)=&\frac{1}{2}\omega\sum_{i=1}^{N}\frac{dV_{uv}(\alpha_i)}{d\alpha}\left[sign\left(dV_{uv}(\alpha_i)\right)-1\right]\\&+\frac{1}{2}\omega\sum_{i=1}^{N-1}\frac{dV_{bv}(\alpha_i,\alpha_{i+1})}{d\alpha}\left[sign\left(dV_{bv}(\alpha_i,\alpha_{i+1})\right)-1\right]\\&+\frac{1}{2}\omega\frac{dV_{bv}}{d\alpha}(\alpha_N,\alpha_1)\left[sign\left(dV_{bv}(\alpha_N,\alpha_1)\right)-1\right]\end{aligned} \tag{13}$$

2.2.3 Main ring rotation analysis

Force due to pressured oil inside main ring

In this research pump, the eccentricity between the rotor and the ring is maximum (e_{c_max} = R_s - R_r) at the initial state of the main ring. In this case, the rotor contacts with the inner contour of the ring at point C_{10}, and the center point of the ring inner contour is at O_{s0}.

Two coordinate systems have been used which are a Cartesian coordinate system positioning at the rotor center ($O_rX_rY_r$), and a polar coordinate system of which the pole is located at center point of the ring inner contour and the axis points to a point on the ring at which the ring contour is closest to the rotor.

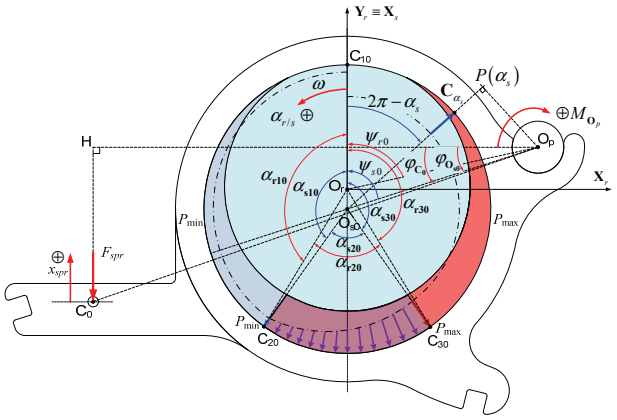

(a) At initial position of main ring

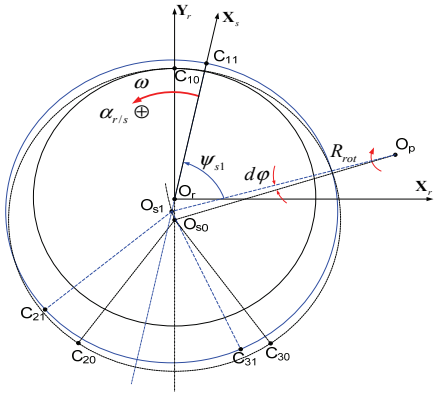

(b) After a small rotation of main ring

Fig. 5 Pressure distribution inside main ring

During the operation, the eccentricity between the rotor and the ring makes a cam contour if considering O_r is the center point. Based on the pump working principle, the pressure distribution profile within one rotation of the pump at the ring initial position (see Fig. 5a) can be divided into three regions: the first region at arc $\overline{C_{10}C_{20}}$ relates to the suction zone (the pressure is the same as the minimum pressure P_{min} or tank pressure); the second region at arc $\overline{C_{20}C_{30}}$ gives the pre-compression for the oil chambers (the pressure increases from P_{min} to P_{max} or outlet pressure); and the third region at arc $\overline{C_{30}C_{10}}$ relates to the delivery zone (the pressure is the same as the maximum pressure P_{max}).

For a small rotation of the ring, $d\varphi$, around the pivot pin O_p, the center point of the ring inner contour is moved from point O_{s0} to point O_{s1}. The three regions of pressured oil are then re-positioned in which points C_{10}, C_{20}, C_{30} are moved to points C_{11}, C_{21}, C_{31}, respectively (see Fig. 5b). The initial coordinate of point O_s (O_{s0}) is easily determined as

$$\begin{cases} \overline{O_pO_{s0}} = R_{rot} \\ \angle HO_pO_{s0} = \varphi_{O_{s0}} \end{cases} \tag{14}$$

Consequently, trajectory of the center point O_s is determined as a rotating vector of which the length is R_{rot} and the angle is $(\varphi_{O_{s0}} - d\varphi)$. Let define the angle difference between the pole axis and the center line $\overline{O_pO_{st}}$ is ψ_{st}. Then the total moment acting on the ring caused by the pressured oil inside the ring to make it rotate around the pivot pin can be computed as

$$\begin{aligned} \sum M_{O_{p\_oil\_inside}} &= \int_0^{\alpha_{C2t}} R_{rot}\sin(\psi_{st}+\alpha_s)P_{\min}bR_s d\alpha_s \\ &+ \int_{\alpha_{C2t}}^{\alpha_{C3t}} R_{rot}\sin(\psi_{st}+\alpha_s) \\ &\quad \times\left[(P_{\max}-P_{\min})\frac{\alpha_s-\alpha_{C2t}}{\alpha_{C3t}-\alpha_{C2t}}+P_{\min}\right]bR_s d\alpha_s \\ &+ \int_{\alpha_{C3t}}^{2\pi} R_{rot}\sin(\psi_{st}+\alpha_s)P_{\max}bR_s d\alpha_s \end{aligned} \tag{15}$$

Force due to pressured oil outside main ring (through the control orifice)

Considering the oil chamber outside the ring through the control orifice (see Fig. 1), the relationship between input and output flow rates during a small rotation of the ring, $d\varphi$, can be expressed as

$$Q_{\text{inflow}} - Q_{\text{outflow}} = \frac{V_{out}}{\beta_{\text{oil}}}\frac{dP_{\text{out}}}{dt} \tag{16}$$

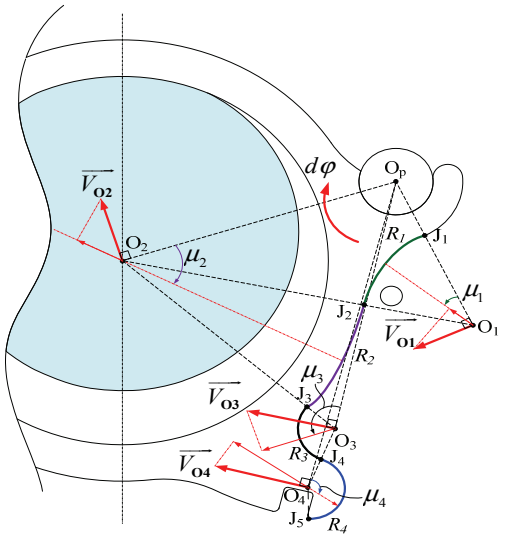

(a) Motion analysis of main ring

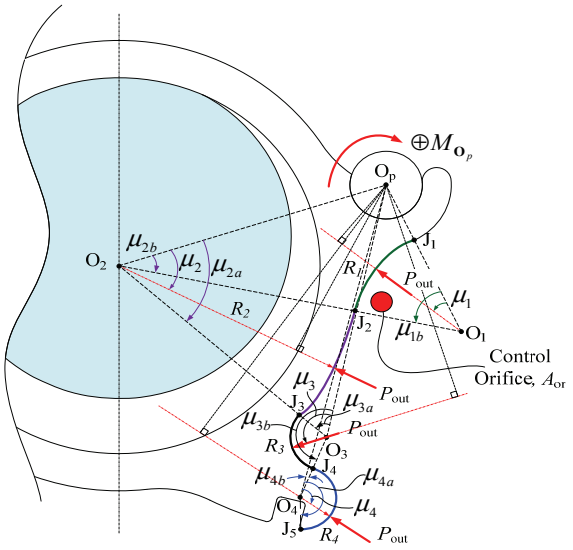

(b) Pressure analysis at outside chamber

Fig. 6 Pressure distribution outside main ring

where: Q_{inflow} and Q_{outflow} are the input and output flow rates computed correspondingly by (17) and (18); V_{out} is the chamber volume which can be measured accurately by using the pump design software; β_{oil} is

Bulk modulus; dP_{out} is the pressure derivation.

$$Q_{\text{inflow}} = C_{\text{or}} A_{\text{or}} \sqrt{\frac{2}{\rho_{\text{oil}}}\left(P_{\max} - P_{\text{out}}\right)} \tag{17}$$

where: $C_{\text{or}}, A_{\text{or}}, \text{and}\, \rho_{\text{oil}}$ are in turn flow coefficient, area of the orifice, and mass density of oil.

$$\begin{aligned} Q_{\text{outflow}} = &-\int_{\mu_{1a}}^{\mu_{1b}} \left(\overline{\text{O}_\text{p}\text{O}_1} d\varphi \sin\mu\right) b R_1 d\mu \\ &-\int_{\mu_{3a}}^{\mu_{3b}} \left(\overline{\text{O}_\text{p}\text{O}_3} d\varphi \sin\mu\right) b R_3 d\mu \\ &+\int_{\mu_{2a}}^{\mu_{2b}} \left(\overline{\text{O}_\text{p}\text{O}_2} d\varphi \sin\mu\right) b R_2 d\mu \\ &+\int_{\mu_{4a}}^{\mu_{4b}} \left(\overline{\text{O}_\text{p}\text{O}_4} d\varphi \sin\mu\right) b R_4 d\mu \end{aligned} \tag{18}$$

The total moment acting on the ring outer surface caused by the pressured oil to make it rotate around then pivot pin can be obtained as (see Fig. 6)

$$\begin{aligned} \sum M_{O_{p\_oil\_outside}} = &\int_{\mu_{1a}}^{\mu_{1b}} \overline{\text{O}_\text{p}\text{O}_1} \sin\mu P_{\text{out}} b R_1 d\mu \\ &+\int_{\mu_{3a}}^{\mu_{3b}} \overline{\text{O}_\text{p}\text{O}_3}.\sin\mu P_{\text{out}} b R_3 d\mu \\ &-\int_{\mu_{2a}}^{\mu_{2b}} \overline{\text{O}_\text{p}\text{O}_2} \sin\mu P_{\text{out}} b R_2 d\mu \\ &-\int_{\mu_{4a}}^{\mu_{4b}} \overline{\text{O}_\text{p}\text{O}_4} \sin\mu P_{\text{out}} b R_4 d\mu \end{aligned} \tag{19}$$

Force due to centrifugal effects of vanes and oil volumes between vanes

Centrifugal force generated by an oil chamber between each two consecutive vanes is firstly analyzed in Fig. 7. The centrifugal force of this chamber is presented by a vector $F_{oil\_cen}(i)$ positioning at the chamber mass center G_i which can be presented by

$$\xi = \frac{\overline{\text{G}_i\text{W}_1}}{\overline{\text{G}_i\text{Q}}} = \frac{S_{\text{A}_{it}\text{A}_{it}^*\text{A}_{(i+1)t}}}{S_{\text{A}_{it}\text{A}_{it}^*\text{MN}}} \tag{20}$$

where: W_1 and Q are the mass centers of the $\text{A}_{it}\text{A}_{it}^*\text{MN}$ and $\text{A}_{it}\text{A}_{it}^*\text{A}_{(i+1)t}$ blocks, respectively; and:

$$\begin{cases} S_{\text{A}_{it}\text{A}_{it}^*\text{A}_{(i+1)t}} = \dfrac{1}{2}\left(\beta_i - \beta_{i+1}\right)\left(\rho_{i+1} - \rho_i\right) \\ S_{\text{A}_{it}\text{A}_{it}^*\text{MN}} = \left(\beta_i - \beta_{i+1}\right)\left(\rho_i - R_r\right) \end{cases} \tag{21}$$

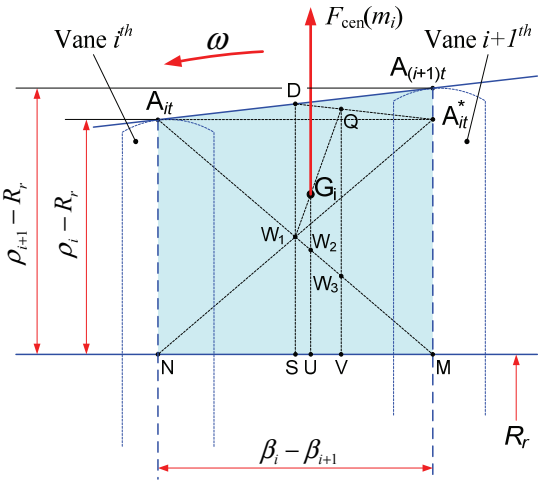

Fig. 7 Centrifugal force generated by an oil

chamber volume between two consecutive vanes

By using simple calculation, the following relation can be obtained:

$$\begin{cases} \overline{\text{G}_i\text{U}} = \dfrac{\xi}{1+\xi} \times \dfrac{\rho_i + \rho_{i+1} - 2R_r}{3} + \dfrac{3+2\xi}{3+3\xi} \times \dfrac{\rho_i - R_r}{2} \\ \overline{\text{UM}} = \dfrac{3+2\xi}{3+3\xi} \times \dfrac{\beta_i - \beta_{i+1}}{2} \end{cases} \tag{22}$$

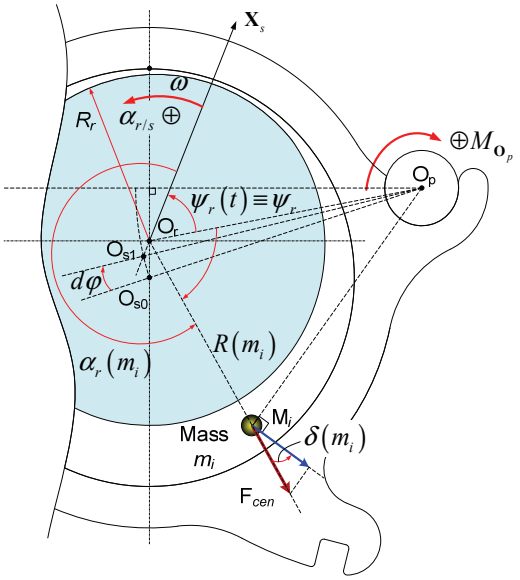

Fig. 8 Centrifugal force effect on ring rotation

From (22), the coordinate of G_i is finally calculated as

$$\begin{cases} \overline{\text{O}_r\text{G}_i} = R_r + \overline{\text{G}_i\text{U}} \\ \angle\left(\overrightarrow{\text{O}_r\text{X}_s}, \overrightarrow{\text{O}_r\text{G}_i}\right) \equiv \alpha_r\left(G_i\right) \equiv \alpha_r\left(\text{A}_i\text{A}_{(i+1)}\text{MN}\right) \\ \qquad = \beta_{i+1} + \dfrac{3+2\xi}{3+3\xi} \times \dfrac{\beta_i - \beta_{i+1}}{2} + \pi \end{cases} \tag{23}$$

Centrifugal force of an object of mass m_i travelling in a circle with radius $R(m_i)$ around the rotor center can be computed as (see Fig. 8)

$$F_{cen}(m_i) = m_i \omega^2 R(m_i) \tag{24}$$

where: m_i and $R(m_i)$ are defined as in equation (25), (26) and (27) corresponding to an oil chamber between two consecutive vanes, an oil chamber under each vane and a vane.

$$\begin{cases} m_i = \left(S_{\mathrm{A}_{it}\mathrm{A}^*_{it}\mathrm{A}_{(i+1)t}} + S_{\mathrm{A}_{it}\mathrm{A}^*_{it}\mathrm{MN}} \right) \times b \times \rho_{\mathrm{oil}} \\ R(m_i) = \overline{\mathrm{O}_r\mathrm{G}_i} \end{cases},$$
$$\left(\text{for an oil chamber between two consecutive vanes}\right) \tag{25}$$

$$\begin{cases} m_i = t_v \times \left(R_r - R_{rv} + l_{vi} - h_v \right) \times b \times \rho_{\mathrm{oil}} \\ R(m_i) = R_{rv} + \left(R_r - R_{rv} + l_{vi} - h_v \right)/2 \end{cases},$$
$$\left(\text{for an oil chamber under a vane}\right) \tag{26}$$

$$\begin{cases} m_i = t_v \times h_v \times b \times \rho_{\mathrm{steel}} \\ R(m_i) = l_{vi} + R_r - h_v/2 \end{cases}, \left(\text{for a vane}\right) \tag{27}$$

where: h_v is the length of vane; ρ_{steel} is mass density of vane material – steel.

The total moment acting on the ring caused by the centrifugal forces of N vanes and N oil chambers are derived as

$$\sum M_{O_{p\_cen}} = -\sum_{i=1}^{N} F_{cen}(m_i) \times \cos\left(\delta(m_i)\right) \times \overline{\mathrm{O}_\mathrm{p}\mathrm{M}_i} \tag{28}$$

$$\overline{\mathrm{O}_\mathrm{p}\mathrm{M}_i} = \sqrt{\overline{\mathrm{O}_\mathrm{p}\mathrm{O}_\mathrm{r}}^2 + R^2(m_i) - 2\overline{\mathrm{O}_\mathrm{p}\mathrm{O}_\mathrm{r}} R(m_i) \cos\left(\alpha_r(m_i) + \psi_r\right)} \tag{29}$$

$$\delta(m_i) = \frac{\pi}{2} + \mathrm{asin}\left[\frac{\overline{\mathrm{O}_\mathrm{p}\mathrm{O}_\mathrm{r}}}{\overline{\mathrm{O}_\mathrm{p}\mathrm{M}_i}} \sin\left(\alpha_r(m_i) + \psi_r\right) \right] \tag{30}$$

Force of compression spring

From Fig. 5, the moment generated by the spring force can be computed as

$$M_{O_{spr}} = -F_{spr} \times \overline{\mathrm{O}_\mathrm{p}\mathrm{H}} \cos(\varphi_C) \tag{31}$$

where: $\overline{\mathrm{O}_\mathrm{p}\mathrm{H}}$ is a constant obtained based on distance $\overline{\mathrm{O}_\mathrm{p}\mathrm{C}_0}$ and angle φ_{C_0} defined when the ring is at the initial position; $\varphi_C = \varphi_{C_0} - d\varphi$; and F_{spr} is derived as

$$F_{spr} = F_{spr0} + k_{spr} x_{spr};$$
$$\left(F_{spr0} \text{ is pre-load force of the spring at initial position}\right) \tag{32}$$

$$x_{spr} = \overline{\mathrm{O}_\mathrm{p}\mathrm{H}} \left(\tan(\varphi_C) - \tan\left(\varphi_{C_0}\right) \right) \tag{33}$$

Finally, the ring rotation defined by summing moments acting on the ring around the pivot point:

$$I_{ring}\ddot{\varphi} = \sum M_{O_{p\_oil\_inside}} + \sum M_{O_{p\_oil\_outside}} + \sum M_{O_{p\_cen}} + M_{O_{spr}} \tag{34}$$

here: I_{ring} is the ring moment of inertia.

3. Modeling results

3.1 Modeling process

In this section, numerical simulations and analyses have been carried out based on the vane pump model developed in Section 2 in order to evaluate the working performance of the pump. The setting parameters for the pump model were obtained from the designed pump geometric as shown in Table 1. The pump speed was simulated up to 4000rpm.

Table 1: Setting parameters for pump model

Parameter	Unit	Value
Rotor radius, R_r	mm	24
Slot end point – curve radius, R_{rv}	mm	13
Ring inner contour radius, R_s	mm	27.5
Ring depth, b	mm	28
Number of vanes, N		9
Vane dimension: t_v x h_v	mm x mm	2.5 x 10
Spring stiffness, k_{spr}	kgf/mm	4.544
Spring pre loading force, F_{spr0}	kgf	30.8992
Other geometric parameters	$\overline{\mathrm{O}_\mathrm{p}\mathrm{H}} = 80.06\mathrm{mm}; \overline{\mathrm{HC}_0} = 29.7\mathrm{mm};$ $\overline{\mathrm{O}_\mathrm{p}\mathrm{O}_1} = 24\mathrm{mm}; \overline{\mathrm{O}_\mathrm{p}\mathrm{O}_2} = 38.75\mathrm{mm};$ $\overline{\mathrm{O}_\mathrm{p}\mathrm{O}_3} = 38.15\mathrm{mm}; \overline{\mathrm{O}_\mathrm{p}\mathrm{O}_4} = 48.15\mathrm{mm};$ $R_1 = 15\mathrm{mm}; R_2 = 33.25\mathrm{mm};$ $R_3 = 5\mathrm{mm}; R_4 = 5\mathrm{mm};$	
Oil SAE 5W 20 Bulk modulus, β_{oil}	$\mathrm{N/m^2}$	1.5 x 10^9
Oil SAE 5W 20 Density, ρ_{oil}	$\mathrm{kg/m^3}$	852

3.2 Simulation results

First of all, the pump model was tested in the free load condition. In this condition, the suction port was connected from the oil sump and the pumped flow rate was directly return to the oil sump without any restrictor. Fig. 9 then displays an analysis of the first four consecutive vanes as well as the volume derivatives generated by these vanes in case the pump speed and dis-charge pressure are in turn kept at constant values: 500rpm and 1bar.

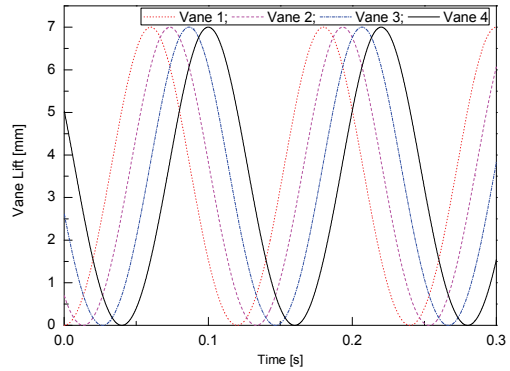

(a) Analysis of vane lifts

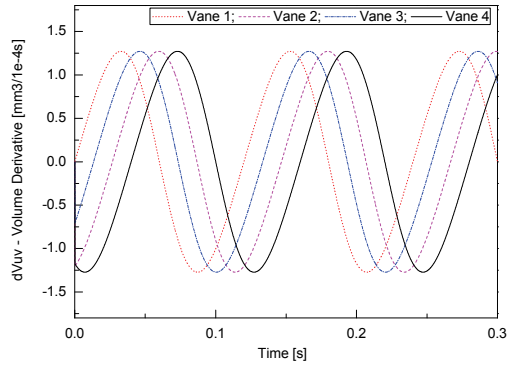

(b) Analysis of volume derivative under vanes

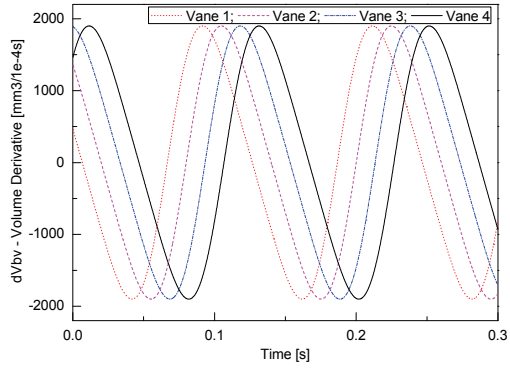

(c) Analysis of volume derivative between vanes

Fig. 9 Analysis of four consecutive vanes

With the counter-clockwise rotation of the rotor shaft, the movements of vanes were obtained as shown in Fig. 9a. Consequently, the volume under each vane and volume between each two vanes generated by the vane lifts were analyzed in figures 9b and 9c, respectively. The vane movement was also checked with different pump speeds while the pressure was still kept at the constant value. The results were then observed and plotted in Fig. 10. From this figure, it is clear that the vanes functioned well in all the conditions.

In vane-type oil pump, if considering that the vane thicknesses is small enough to neglect, the theoretical pump flow rate can be approximately calculated as, Q_{th_app}

$$Q_{th\_app}(\alpha) = \omega b\left(R_s^2 - R_r^2\right) = \frac{\pi n}{30} b\left(R_s^2 - R_r^2\right) \tag{35}$$

To verify the theoretical flow rates produced by employing the proposed theoretical model, the flow rates obtained by (13) with respect to different working speeds are compared with the flow rates approximated by (35). The comparison result is shown in Table 2. From this table, it can be seen that the model functions well in deriving the theoretical pump flow rate.

Table 2: Comparison of theoretical flow rates

Speed [rpm]	1000	2000	3000	4000
Q_{th} from (13) [lpm]	29.335	58.747	88.238	117.815
Q_{th_app} from (35) [lpm]	31.711	63.423	95.134	126.845

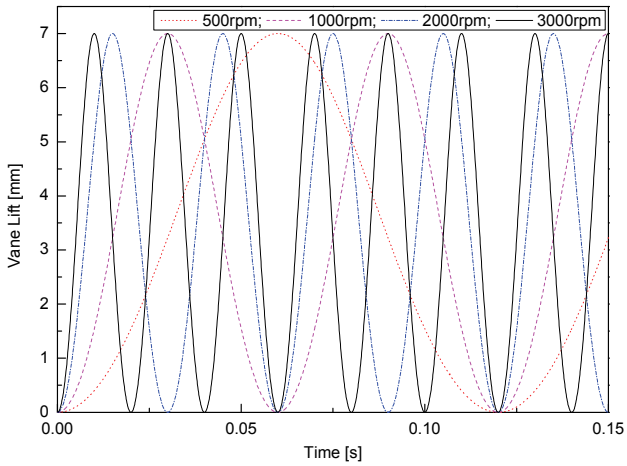

Fig. 10 Analysis of vane movement with respect to different pump speeds

Next, the steady-state flow-pressure characteristic of the pump model was investigated as depicted in Fig. 11. The flow rate was checked at different setting pressure values and different pump speeds in the free-load condition. The flow – pressure characteristic points

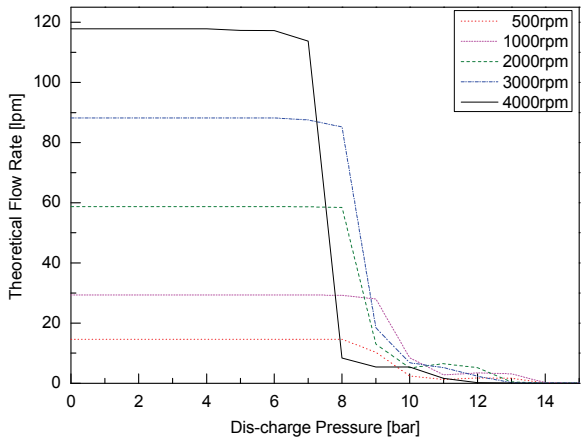

Fig. 11 Steady state flow – pressure characteristic

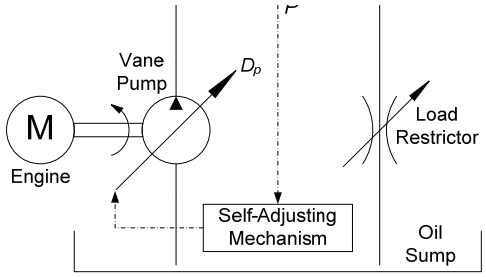

Fig. 12 Simulated lubrication system

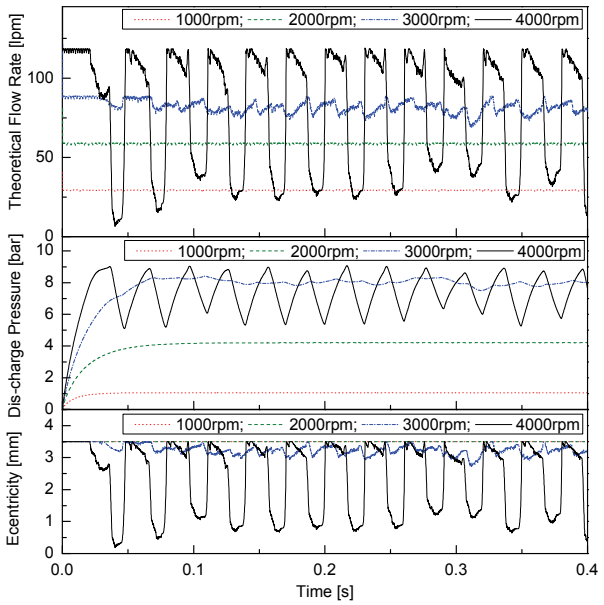

Fig. 13 Performance analysis in constant load condition

out that a higher pressure level is corresponding to a higher reduction of pump displacement, or the higher reduction of pump flow rate. The reason is the significant rising of the force acting on the ring due to pressured oil outside the main ring (see Section 2.2.3b), subsequently degrading the eccentricity of the rotor and the ring inner contour.

As a result, the pump flow rate is decreased and becomes to zeros when the ring inner contour center coincides with the rotor center.

Finally, the pump model was tested in case of connecting the pump delivery port to a load component before returning to the oil pump. In this case, the load is simulated as a fixed flow restriction valve (orifice) as depicted in Fig. 12. The valve could allow the flow rate with maximum of 135 lpm corresponding to a 10bar of the pressure drop over this valve. The simulations were performed with three different pump speeds while the valve opened area was set to 80%. The results were then obtained as plotted in Fig.13. It can be seen that with low speeds as 1000rpm and 2000rpm, the eccentricity between the rotor and the ring was stable at the initial state (maximum eccentricity) (see the bottom sub-plot in Fig.13). It is because the low speeds performed corresponding low delivering flow rates which were fully allowed to pass through the restriction valve. The delivering pressures in these cases were then quite low (see the middle sub-plot in Fig. 13). Since, the total generated moment around the pivot pin was not enough to make the ring rotate. Only when the speed was increased as 3000rpm and 4000rpm, the pumped flow rate was over the capacity of the restrictor, consequently causing a rising in the delivering pressure. This high pressure level created the moment around the pivot pin largely enough to rotate the ring. As a result, the eccentricity was automatically changed to the steady-state position to adjust the delivering flow. The pump operation in this case can be seen clearly in Fig. 13 with the dash-dot-blue and solid-black lines. The results prove that the pump has enough ability in auto-adjusting the displacement with respect to each working condition.

4. Conclusions

The mathematical model of a typical variable displacement vane-type oil pump for lubrication systems has been presented in this paper. By employing the displacement control mechanism based on the working pressure and the balance spring, the lubricating oil can be easily and continuously adjusted with respect to the desired performance to obtain the highest lubricating efficiency. A variable displacement vane-type oil pump made by MyungHwa Co. Ltd. has been investigated. Consequently, the mathematical model and theoretical flow rate of this pump was developed and analyzed based on its design and dynamic analyses. Finally, numerical simulations have been carried out to investigate the working performance of the designed pump model. The simulation results show that the pump could adapt well with any engine lubrication requirement. This variable displacement vane-type oil pump with the developed model may become an advanced solution for industrial machines with lubrication purpose in the near future.

Acknowledgements

This research was financially supported by the Ministry of Education, Science Technology (MEST) and National Research Foundation of Korea (NRF) through the Human Resource Training Project for Regional Innovation.

References

1) Rexroth variable displacement vane-type oil pump - http://www.bosch Rexroth.com
2) Atos variable displacement vane-type oil pump - http://www.atos.com
3) Scoda variable displacement vane-type oil pump - http://www.scoda.it
4) Magna Powertrain Inc., Continuously variable displacement vane pump and system, Patent No.: WO 2007/128106 A1, 2007.
5) Magna Powertrain Inc., Variable Capacity vane pump with force reducing chamber on displacement ring, Patent No.: US 2009/0074598 A1, 2009.
6) Magna Powertrain Inc., Variable capacity vane pump with dual control chambers, Patent No.: US 7794217 B2, 2010.
7) D.R. Staley and B.K. Pryor, Pressure regulating variable displacement vane pump, Patent No.: US 7862306 B2, 2011.
8) A. Giuffrida and R. Lanzafame, "Cam shape and theoretical flow rate in balanced vane pumps," Mechanism and Machine Theory, Vol. 40, pp. 353-369, 2005.
9) D.R. Staley, B.K. Pryor and K. Gilgenbach, "Adaptation of a Variable Displacement Vane Pump to Engine Lube Oil Applications," SAE Technical Paper 2007-01-1567, pp. 1-9, 2007.
10) S. Loganathan, S. Govindarajan, J.S. Kumar, K. Vijayakumar and K. Srinivasan, "Design and Development of Vane Type Variable flow Oil Pump for Automotive Application," SAE Technical Paper 2011-28-0102, pp. 1-7, 2011.
11) C. Kim, D.Q. Truong, N.T. Trung, K.K. Ahn, J.I. Yoon, J.S. Lee, H.S. Han and J.B. Kim, "Development of an Electronic Control Variable Displacement Lubrication Oil Pump," Proc. of the 15th International Conference on Mechatronics Technology, Melbourne, Australia, paper 65, 2011.
12) MyungHwa variable displacement vane-type oil pump - http://www.myunghwa.com/